www.sciencemag.org/cgi/content/full/aas9699/DC1

Supplementary Materials for

High-resolution cryo-EM analysis of the yeast ATP synthase in a lipid membrane

Anurag P. Srivastava,* Min Luo,* Wenchang Zhou, Jindrich Symersky, Dongyang Bai, Melissa G. Chambers, José D. Faraldo-Gómez, Maofu Liao,† David M. Mueller†

*These authors contributed equally to this work.
†Corresponding author. Email: david.mueller@rosalindfranklin.edu (D.M.M.); maofu_liao@hms.harvard.edu (M.L.)

Published 12 April 2018 on *Science* First Release
DOI: 10.1126/science.aas9699

This PDF file includes:

Supplementary Text
Figs. S1 to S12
References

Supplementary Text

Choosing Nanodisks For This Study. We chose to use nanodiscs over detergent for a number of reasons. First, we knew that many groups were working on the structure of the ATP synthase by cryo EM and that they were having difficulties in improving the resolution of the structure. We chose not to follow the same protocol that others were using realizing that we might encounter the same issues. Dr. Liao used nanodiscs successfully for the structure determination of other membrane proteins and thus, this experience motivated us to chose nanodiscs over detergent. Second, in principle, the enzyme incorporated into nanodiscs is more native than detergents. This may be the reason why we see Glu59 in an "open" conformation while it is "closed" in detergent. (The "open" conformation we saw in our studies with the yeast c_{10}-ring was under detergent free conditions as well. We were never able to convert the side chains from open to closed further suggesting that the "open" conformation is not allowed under a number of conditions.) Third, we were interested in obtaining structures of inhibitors bound to the enzyme and recognized that the inhibitors bound to the surface of the c_{10}-ring. If we wanted to mimic the structure of the inhibitor binding in the native membrane, then nanodiscs was the preferred system. However, the cryo density associated with the lipids can create a surface density which can make it more difficult to view ligands that bind to the lipid exposed surface of the protein – in this case, oligomycin. Notwithstanding this, we chose nanodisks over detergent for the our studies.

Fig. S1. Composite images of the yeast F_1F_o ATP synthase used in this study. A. Schematic of the design of the fusion construct. **B**. Polypeptide composition of the ATP synthase from wild type (wt) yeast and the strain containing the fusion construct of subunits F6 and δ.

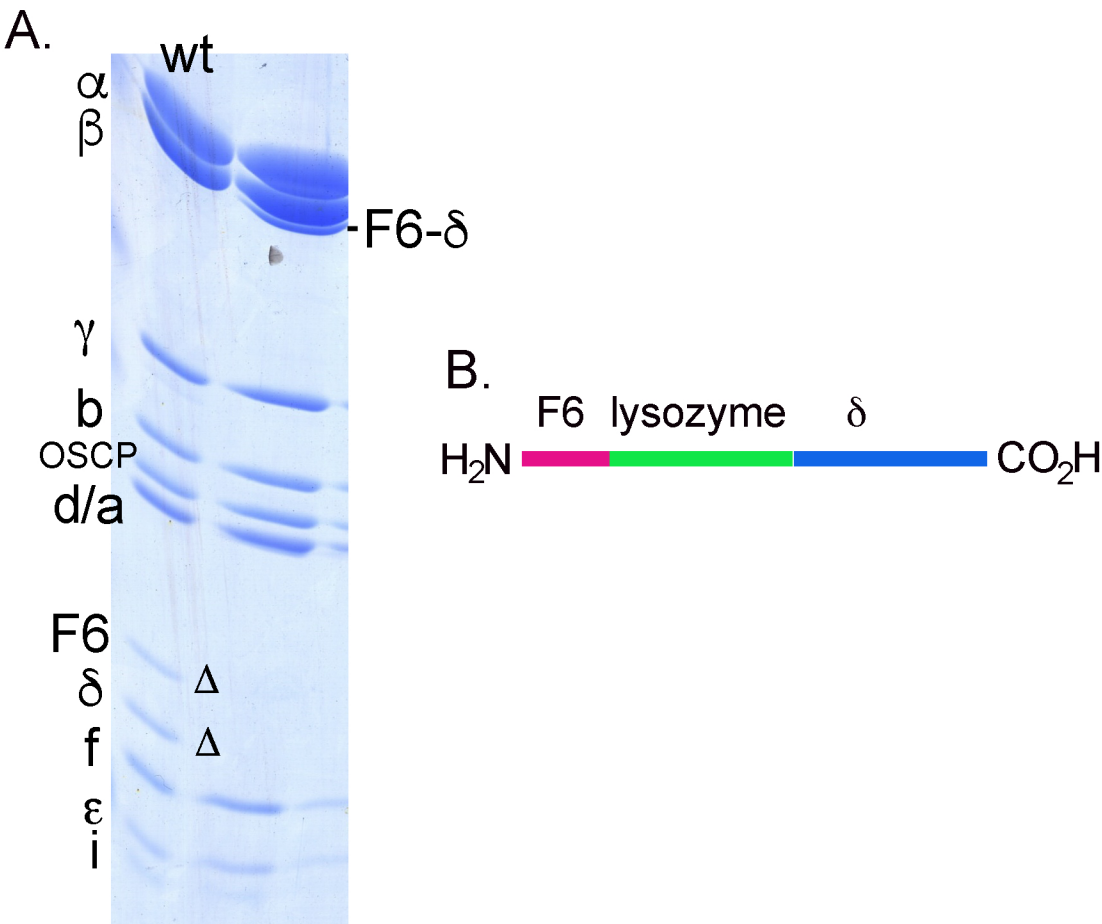

Fig. S2. Single-particle cryo-EM analysis of ATP synthase in nanodiscs. A. Representative cryo-EM image with several particles marked by circles. **B.** 2D averages of cryo-EM particles. The box dimension is 394 Å. **C.** Image processing workflow. The density of lysozyme ("LZ") is clearly shown in the 3D reconstruction of one 3D class. The final F_1F_o and F_o maps with their overall resolutions are indicated in red boxes.

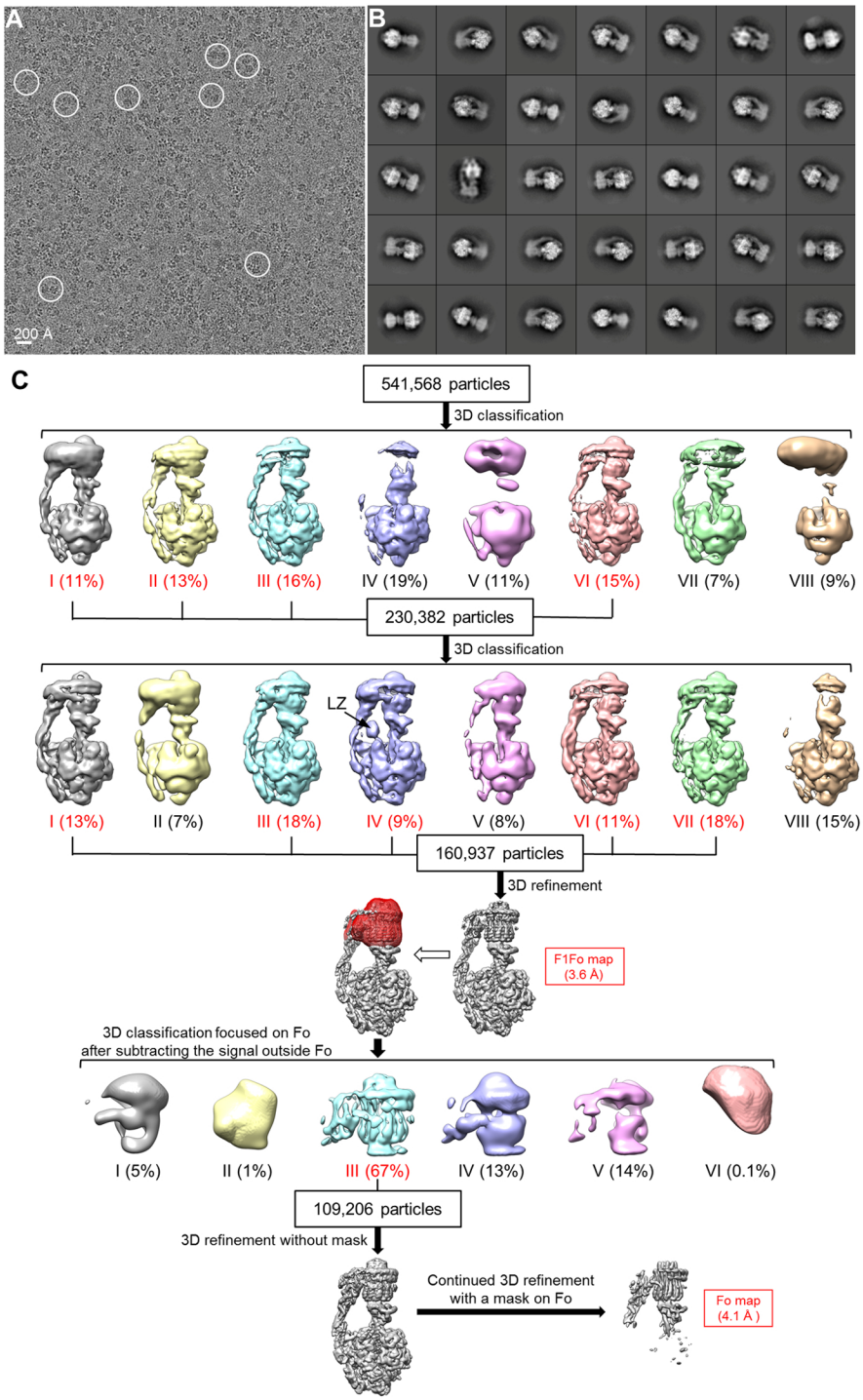

Fig. S3. Single-particle cryo-EM analysis of ATP synthase in nanodiscs with oligomycin. a, Representative cryo-EM image with several particles marked by circles. **b**, 2D averages of cryo-EM particles. The box dimension is 394 Å. **c**, Image processing workflow. The final F_1F_o and F_o maps with their overall resolutions are indicated in red boxes.

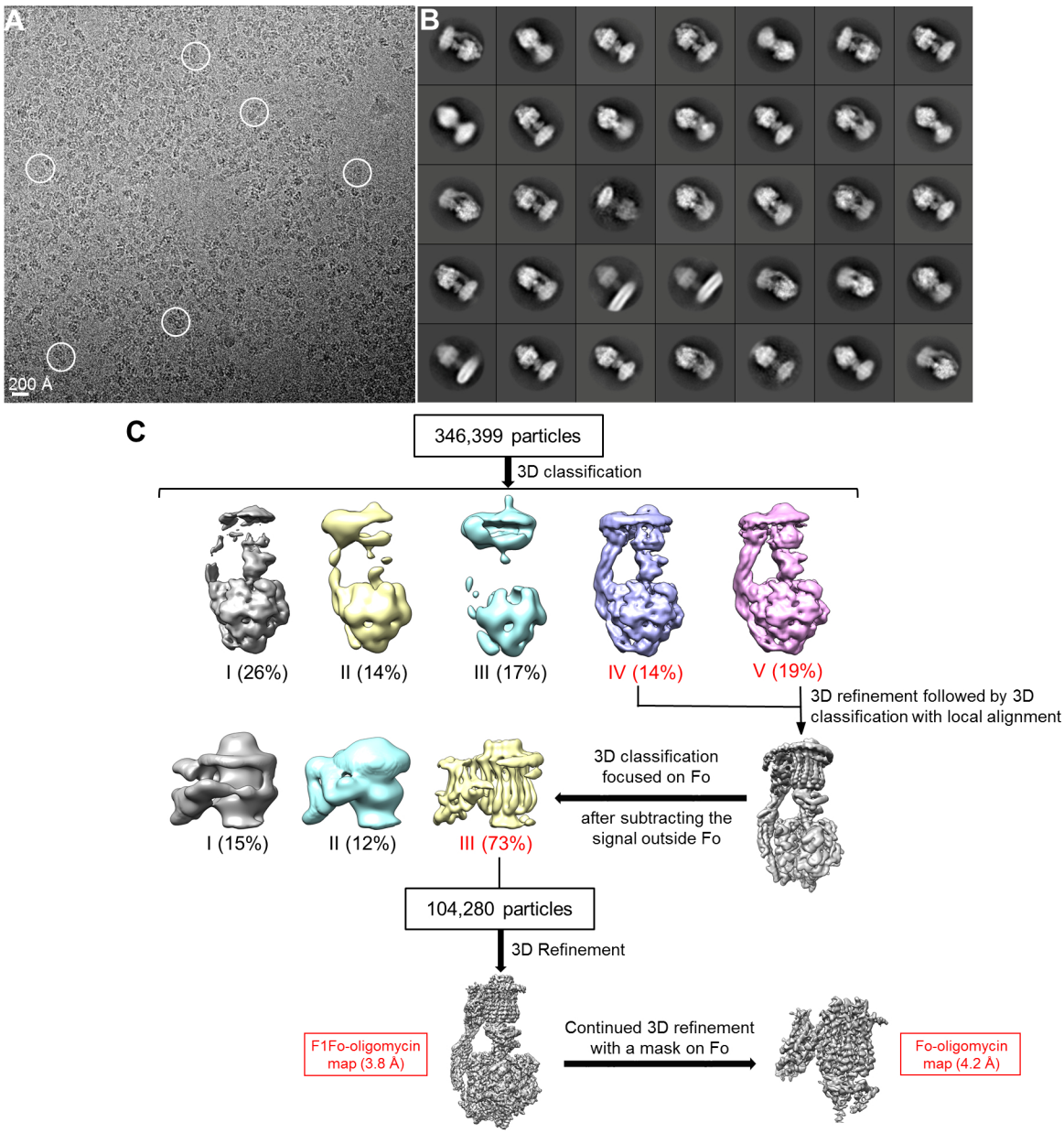

Fig. S4. The analyses of the final cryo-EM maps of F_1F_o (**A**), F_o (**B**), F_1F_o with oligomycin (**C**) and F_o with oligomycin (**D**) are shown in four panels from left to right. First, four Fourier shell correlation (FSC) curves: gold-standard FSC between two half data maps with indicated resolution at FSC=0.143 (black); FSC between atomic model and the final map with indicated resolution at FSC=0.5 (red); FSC between half data map 1 (orange) or half data map 2 (blue) and the atomic model refined against half data map 1. Second, surface and cross-sectional views of the cryo-EM maps filtered to their estimated overall resolution and colored according to local resolution. Third, histogram of voxels with different resolutions. Four, angular distribution of the cryo-EM particles included in the final 3D reconstruction.

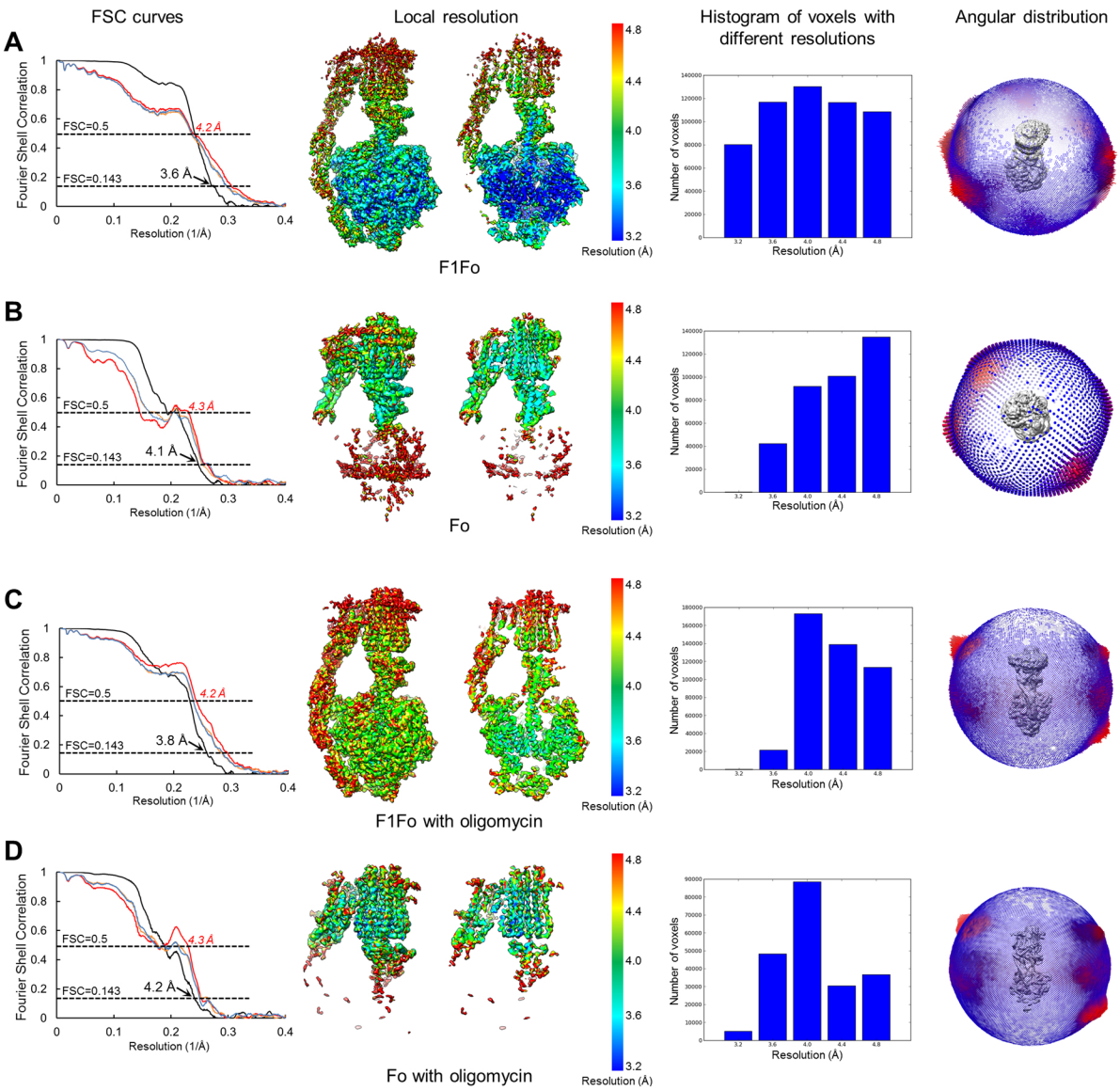

Fig. S5. Examples of the fit of the models and the cryo-EM maps.

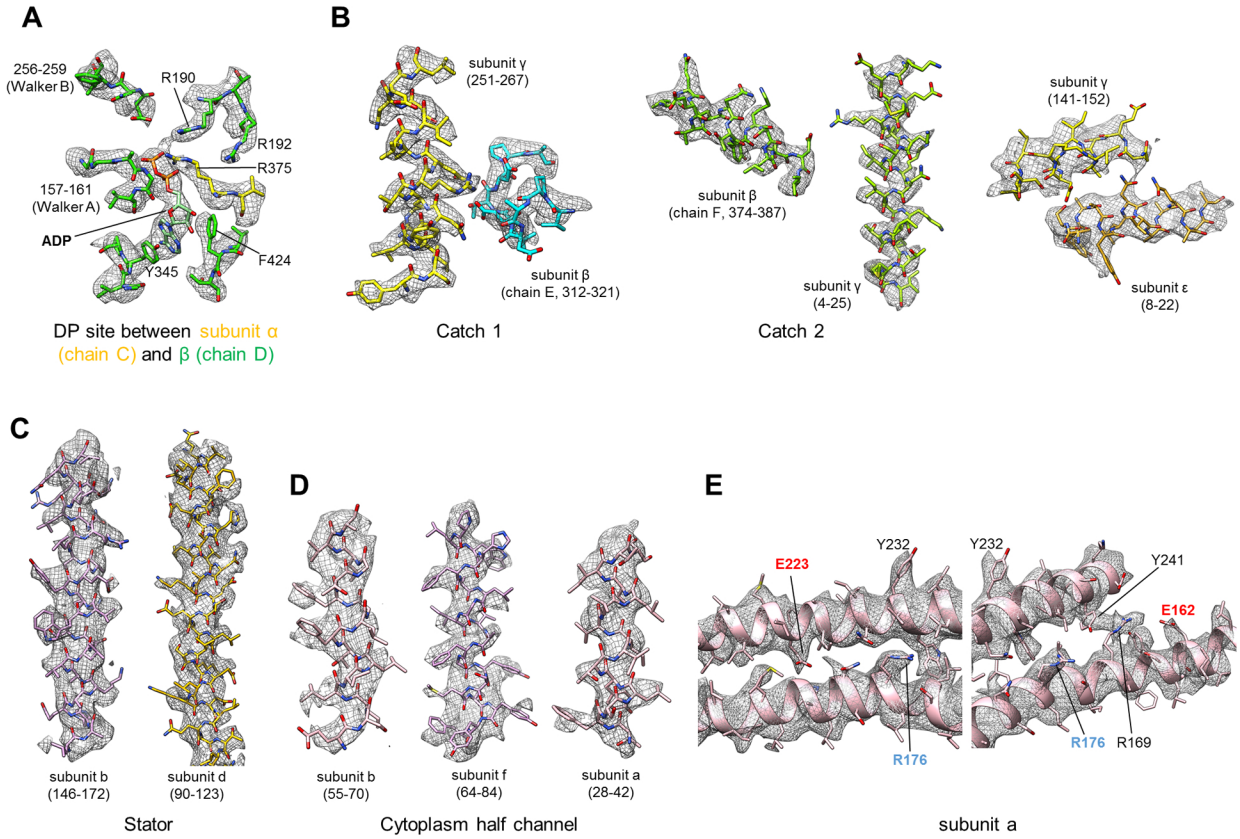

Fig. S6. EM density and atomic model of c_{10}-ring. A. Cross-sectional view of the final F_o map at the level of Glu59 residues in subunit c (left) and side views of the EM density of four c subunits superimposed on the atomic model (right). The cross section is parallel to the membrane plane and viewed from the side of the intermembrane space. The subunits a and c are colored yellow and green, and the ten c subunits are numbered. **B.** same as **A**, except for the final F_o map with oligomycin.

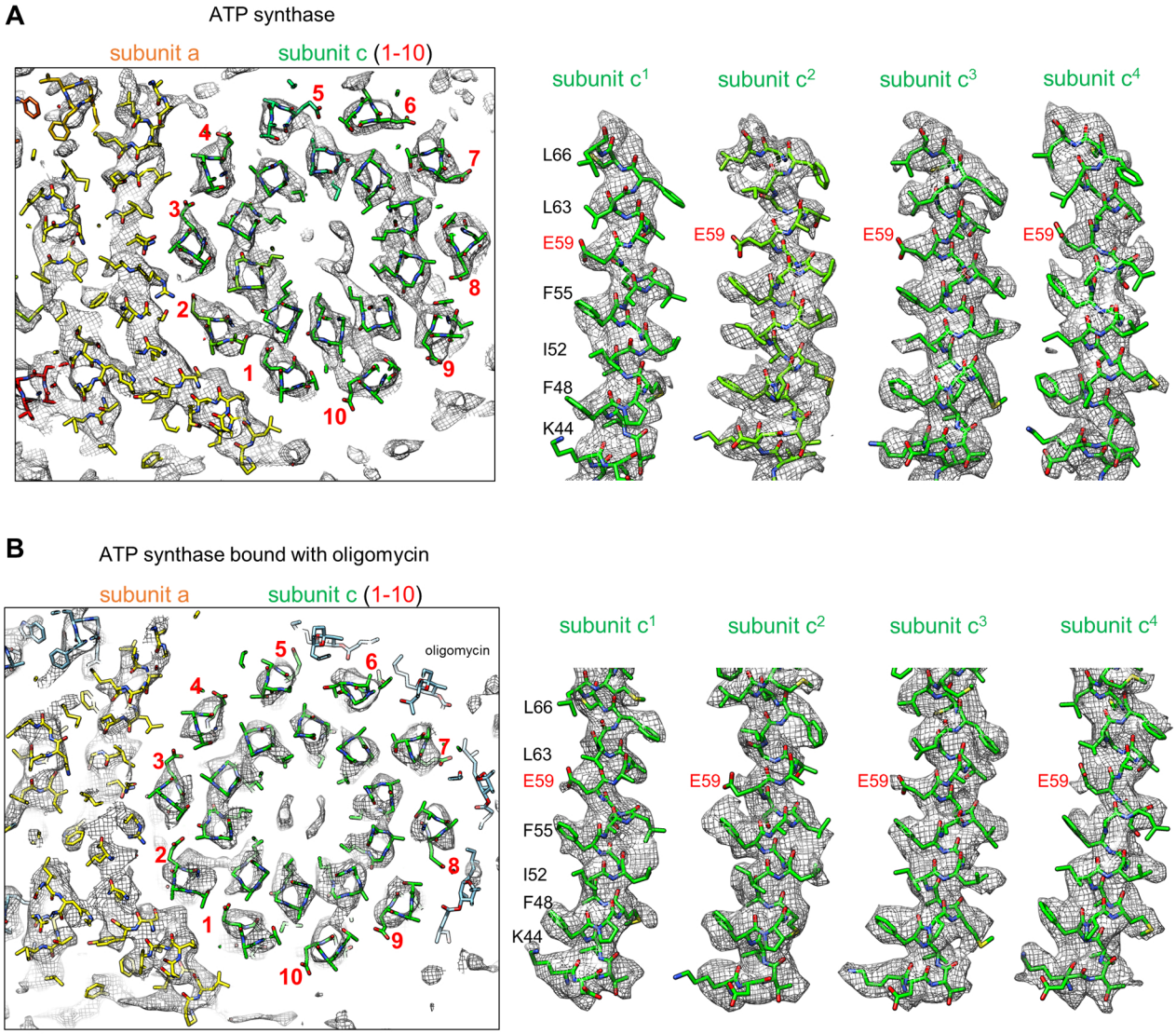

Fig. S7. Interaction of the N-terminal residues of the α-subunits with the stator. A. major sites of interaction between the α-subunit and the stator. Shown is an image of F_1F_o without the β-subunits and interacting regions of the α-subunits with the stator, labeled as I-III (IV is not clearly visible from this view). The residues that are within 4Å of residue within one of the three α-subunits are shown as spheres. **B.** Expanded view of **A**. with arrows identifying the interacting regions. **C.** Back view of A. and expanded to see region IV. Note that OSCP is at the top colored blue. Key: chains A, B, and C make α_E, α_{TP}, and α_{DP}, respectively.

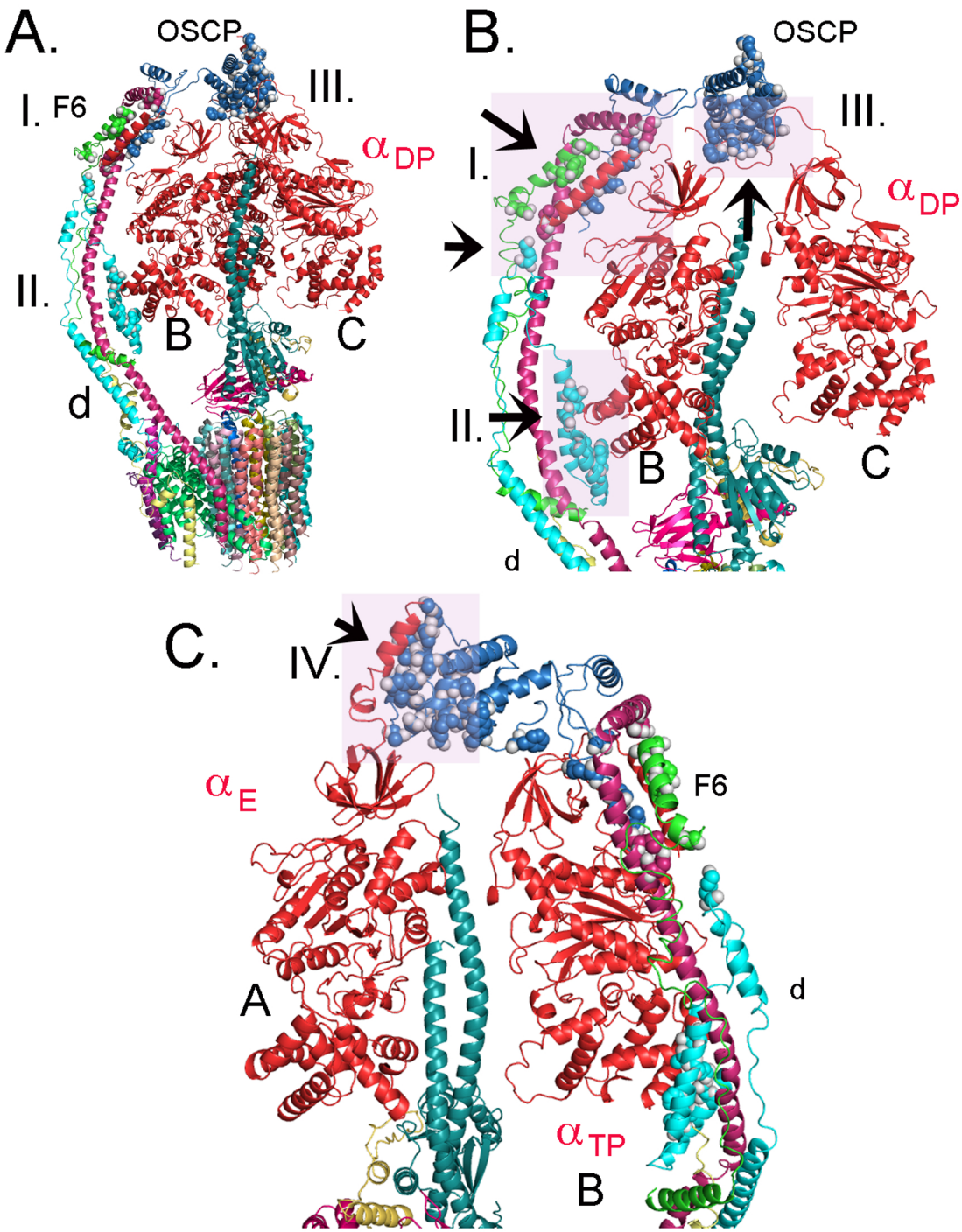

Fig. S8. The carboxyl side chain of c-Glu59 in the open position in the membrane phase. Shown is a top view (matrix side) of the c_{10}-ring of native F_1F_o and a-subunit (numbered 1-10, with 1 being the first subunit with interactions with a-subunit and numbered in the direction of rotation during ATP synthesis). The c_{10}-ring was superimposed with the c_{10}-ring from the crystal structure (pdb: 3U2F) where c-Glu59 is in the "open" conformation (shown in turquoise). In 4 instances (labeled as "O"; c^4, c^6, c^9, c^{10}), the carboxyl side chain of c-Glu59 (magenta) is in the open position based on the electron density here, shown at 2σ. The inset shows an expanded side-view of c^6Glu59 with the density at 2.6σ.

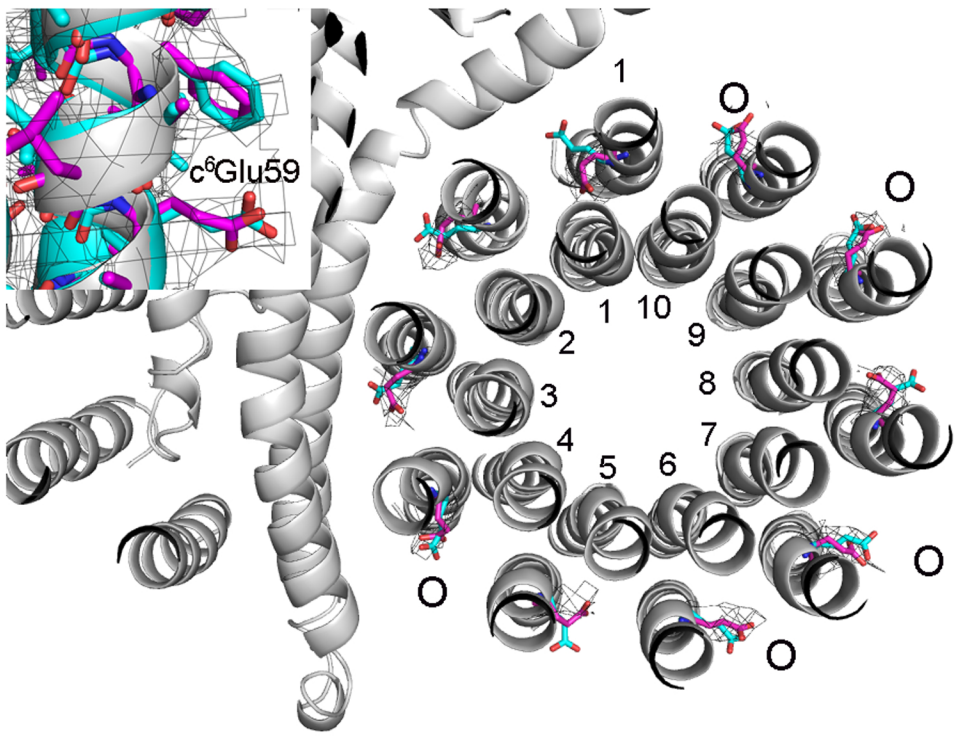

Fig. S9. **Primary sequence alignment of a-subunit.** Sequence alignment using COBALT of the primary sequence of a-subunit. The residues colored in green identify critical residues with the magenta identifying residues that are replaced or replace the critical residues. *Saccharomyces cerevisiae (*P00854), *Mycobacterium tuberculosis* (P9WPV7)*, Escherichia coli* (Q8FBS8)*, Penicillium chrysogenum* (Q36918)*, Drosophila melanogaster* (A0A0M4FZ99), *Homo sapiens* (P00846), *Rattus norvegicus* (P05504), *Arabidopsis thaliana* (P93298), *Zea mays* (P07925), *Chlorella variabilis* (A0A097P5W0)*, Chara vulgaris* (Q7YAN7).

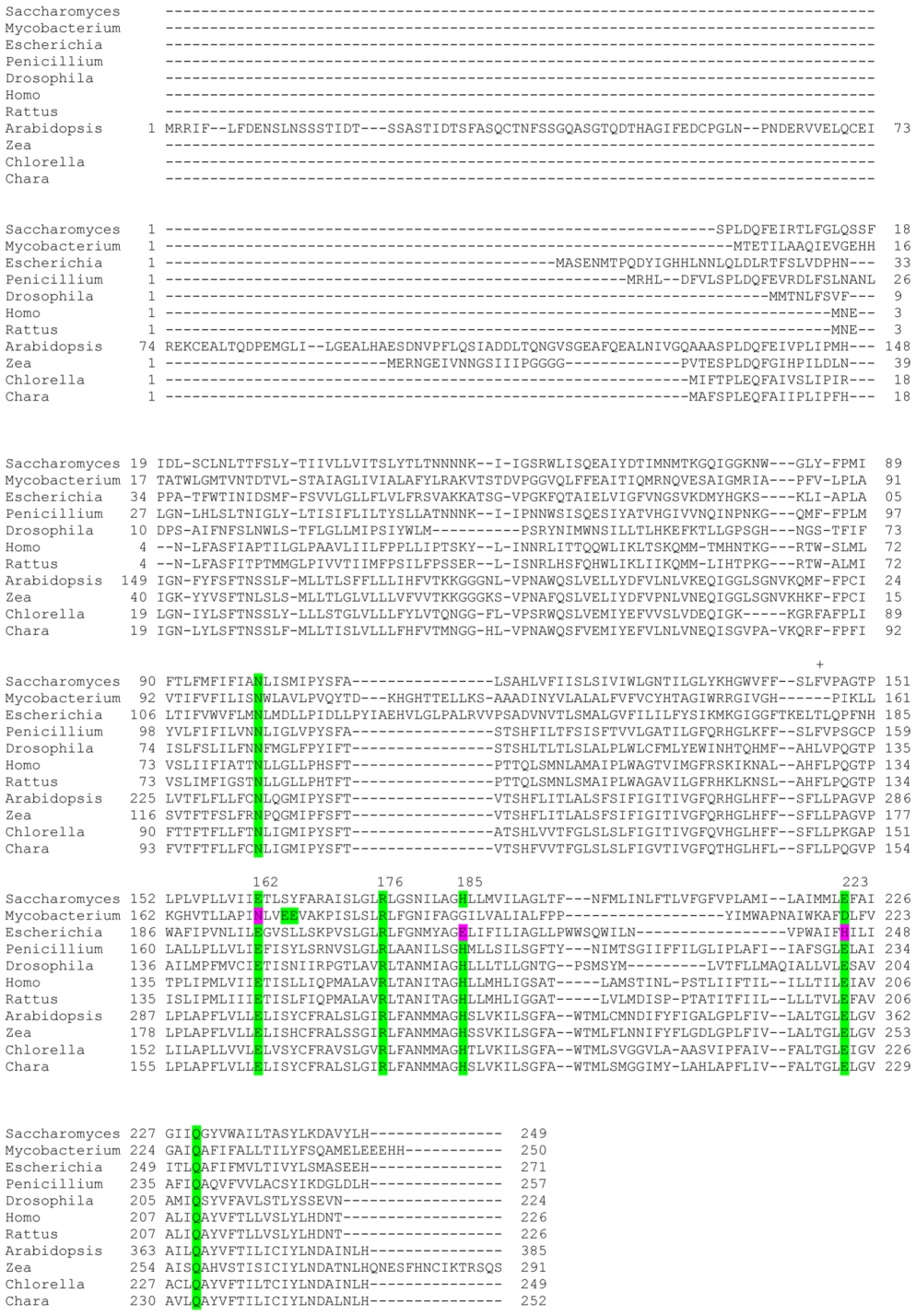

Fig. S10. Rotational states of the c_{10}-ring. The c_{10}-ring was rotated along the z-axis is steps of 9 (yellow), 18 (green) and 27° (blue) relative to the initial state (grey). **A. Top view of the c_{10}-ring in all rotation positions with a-subunit (purple) and the subunits b and f (blue). B. Side view of A. C. Position of c^1Glu59 after rotation of the c_{10}-ring by 9°.** The rotomer of Glu59 is that as observed in c^{10}Glu59, as that is expected to be the conformation as c^{10}Glu59 enters c^1Glu59 space. **D. Position of c^2Glu59 after rotation of the c_{10}-ring by 27°.** The position of Glu59 after rotation of the c_{10}-ring by 27° places the side chain, depending on the rotomer, within 3Å of aAsn180 and 9Å of aGlu223. The distance between Glu59 and aGlu223 is certainly too far for eliciting changes in the chemistry of Glu59, without bridging water molecules or without other conformational changes that might occur during the reaction cycle.

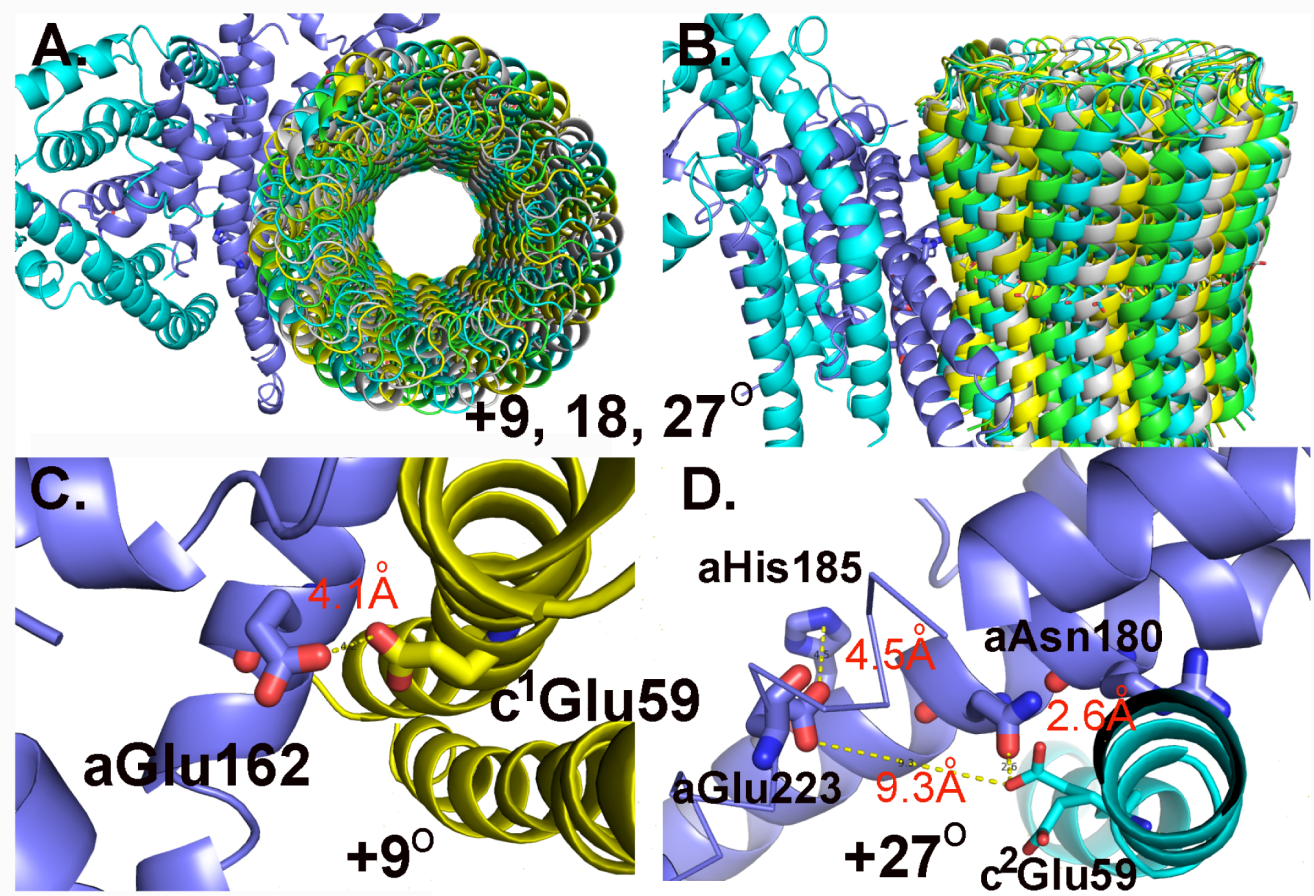

Fig. S11. Structure of "Oligomycin 5" binding site. A. Possible alternate binding mode on the surface of the c^4c^5. Shown in the model of "Oligo5" (turquois) and oligomycin in the standard conformation and binding mode (black). Note cGlu59 does not make any interaction with "Oligo5" and the isopropyl group off C2 is in a much different position. Of the residues on subunit a, only aPro212 is within 4Å of the Oligo5 (not shown). **B. The cryo-EM density corresponding to "Oligo5".** The cryo-EM density at 5.5σ (red) and 4.5σ (black). **B. The cryo-EM density corresponding to Oligo4.** The cryo-EM density at 5.5σ (red) and 4.5σ (black).

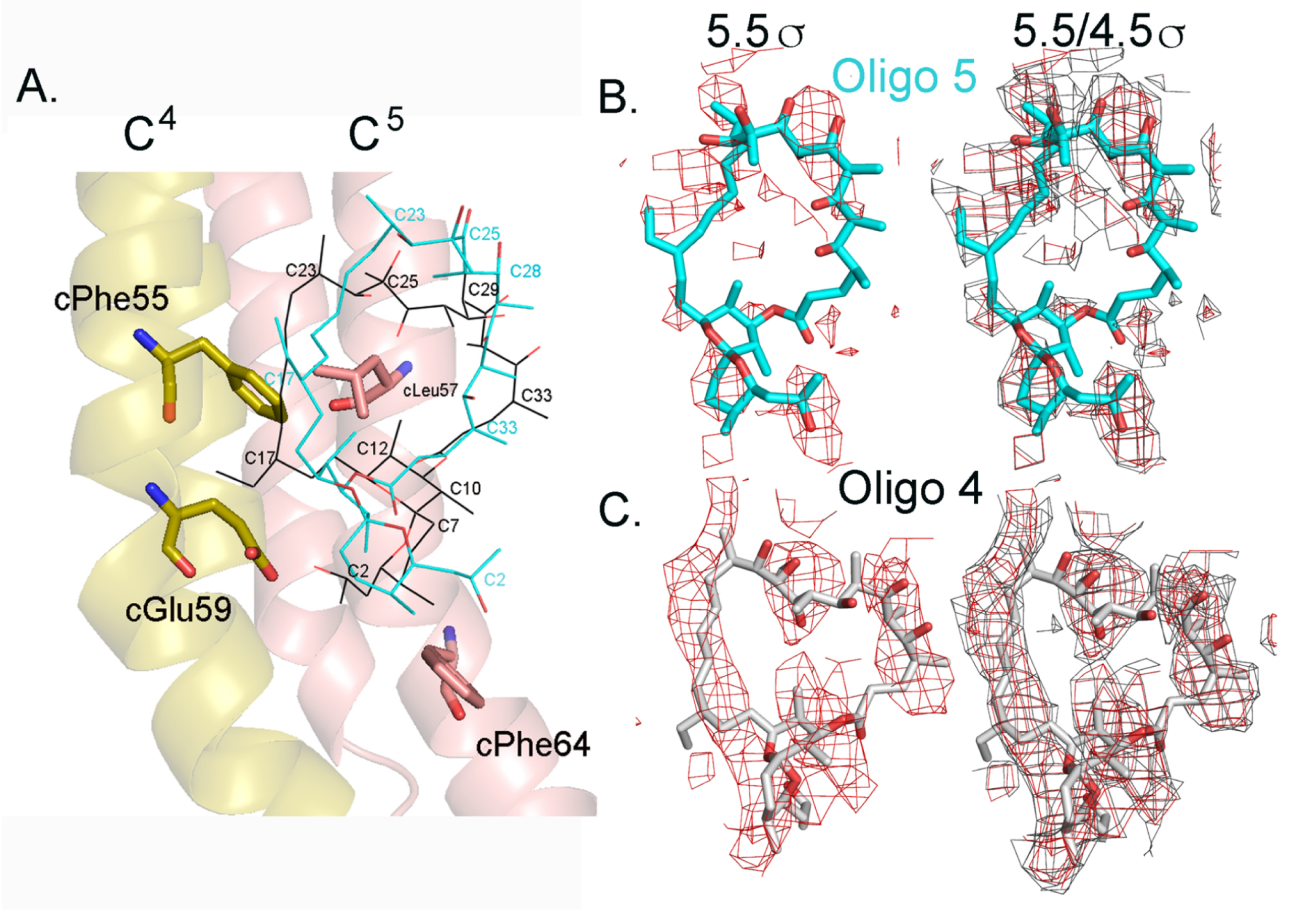

Fig. S12. Molecular dynamics simulations of the c_{10}-ring inhibitor complex in a lipid membrane. **A.** View of the molecular system along the plane of the membrane. In addition to the c_{10}-ring (grey) and the four oligomycin molecules bound (red/magenta/white spheres), the system comprises 227 phospholipid molecules (blue/red/cyan sticks), 17503 water molecules (small red spheres), and 21 mobile ions that neutralize the net charge of the system (orange spheres). The system is approximately 10 x 10 x 10nm^3, for a total of about 95,000 atoms. **B.** Same as (A), viewed from matrix side. Note the interior of the c_{10}-ring is filled with lipid. **C.** Close-up view of oligomycin in the dissociated state.

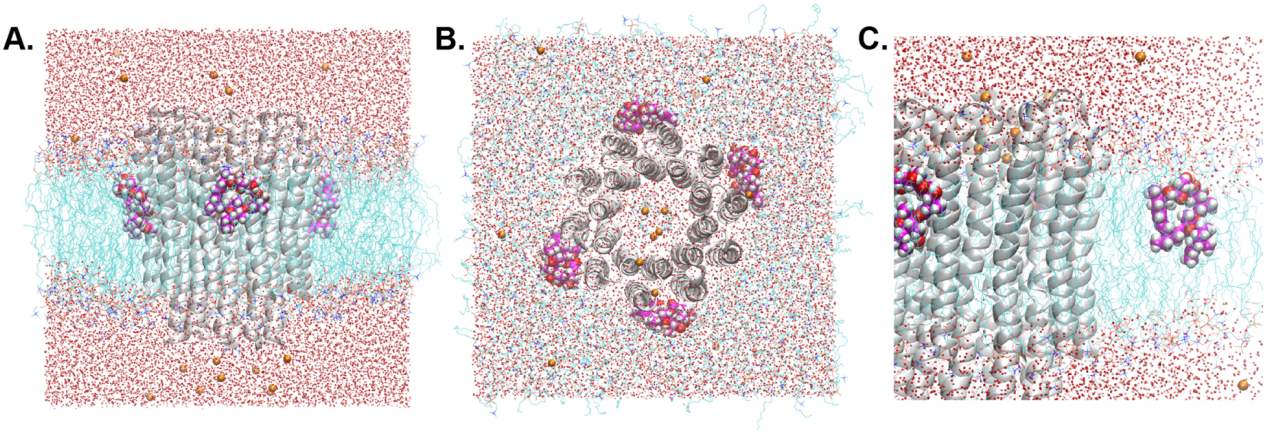

References

1. T. Xu, V. Pagadala, D. M. Mueller, Understanding structure, function, and mutations in the mitochondrial ATP synthase. *Microb. Cell* **2**, 105–125 (2015). doi:10.15698/mic2015.04.197 Medline

2. I. Arnold, K. Pfeiffer, W. Neupert, R. A. Stuart, H. Schägger, Yeast mitochondrial F_1F_0-ATP synthase exists as a dimer: Identification of three dimer-specific subunits. *EMBO J.* **17**, 7170–7178 (1998). doi:10.1093/emboj/17.24.7170 Medline

3. B. Daum, D. Nicastro, J. Austin II, J. R. McIntosh, W. Kühlbrandt, Arrangement of photosystem II and ATP synthase in chloroplast membranes of spinach and pea. *Plant Cell* **22**, 1299–1312 (2010). doi:10.1105/tpc.109.071431 Medline

4. L. A. Baker, I. N. Watt, M. J. Runswick, J. E. Walker, J. L. Rubinstein, Arrangement of subunits in intact mammalian mitochondrial ATP synthase determined by cryo-EM. *Proc. Natl. Acad. Sci. U.S.A.* **109**, 11675–11680 (2012). doi:10.1073/pnas.1204935109 Medline

5. I. G. Denisov, Y. V. Grinkova, A. A. Lazarides, S. G. Sligar, Directed self-assembly of monodisperse phospholipid bilayer nanodiscs with controlled size. *J. Am. Chem. Soc.* **126**, 3477–3487 (2004). doi:10.1021/ja0393574 Medline

6. J. P. Abrahams, A. G. W. Leslie, R. Lutter, J. E. Walker, Structure at 2.8 A resolution of F_1-ATPase from bovine heart mitochondria. *Nature* **370**, 621–628 (1994). doi:10.1038/370621a0 Medline

7. V. Kabaleeswaran, N. Puri, J. E. Walker, A. G. Leslie, D. M. Mueller, Novel features of the rotary catalytic mechanism revealed in the structure of yeast F_1 ATPase. *EMBO J.* **25**, 5433–5442 (2006). doi:10.1038/sj.emboj.7601410 Medline

8. A. Dautant, J. Velours, M. F. Giraud, Crystal structure of the Mg·ADP-inhibited state of the yeast F_1c_{10}-ATP synthase. *J. Biol. Chem.* **285**, 29502–29510 (2010). doi:10.1074/jbc.M110.124529 Medline

9. D. Stock, A. G. W. Leslie, J. E. Walker, Molecular architecture of the rotary motor in ATP synthase. *Science* **286**, 1700–1705 (1999). doi:10.1126/science.286.5445.1700 Medline

10. V. K. Dickson, J. A. Silvester, I. M. Fearnley, A. G. Leslie, J. E. Walker, On the structure of the stator of the mitochondrial ATP synthase. *EMBO J.* **25**, 2911–2918 (2006). doi:10.1038/sj.emboj.7601177 Medline

11. H. Guo, S. A. Bueler, J. L. Rubinstein, Atomic model for the dimeric F_o region of mitochondrial ATP synthase. *Science* **358**, 936–940 (2017). doi:10.1126/science.aao4815 Medline

12. K. R. Vinothkumar, M. G. Montgomery, S. Liu, J. E. Walker, Structure of the mitochondrial ATP synthase from *Pichia angusta* determined by electron cryo-microscopy. *Proc. Natl. Acad. Sci. U.S.A.* **113**, 12709–12714 (2016). doi:10.1073/pnas.1615902113 Medline

13. S. B. Vik, J. C. Long, T. Wada, D. Zhang, A model for the structure of subunit a of the *Escherichia coli* ATP synthase and its role in proton translocation. *Biochim. Biophys. Acta* **1458**, 457–466 (2000). doi:10.1016/S0005-2728 (00)00094-3 Medline

14. S. B. Vik, B. J. Antonio, A mechanism of proton translocation by F_1F_0 ATP synthases suggested by double mutants of the *a* subunit. *J. Biol. Chem.* **269**, 30364–30369 (1994). Medline

15. W. Junge, H. Lill, S. Engelbrecht, ATP synthase: An electrochemical transducer with rotatory mechanics. *Trends Biochem. Sci.* **22**, 420–423 (1997). doi:10.1016/S0968-0004 (97)01129-8 Medline

16. J. Symersky, V. Pagadala, D. Osowski, A. Krah, T. Meier, J. D. Faraldo-Gómez, D. M. Mueller, Structure of the c_{10} ring of the yeast mitochondrial ATP synthase in the open conformation. *Nat. Struct. Mol. Biol.* **19**, 485–491, S1 (2012). doi:10.1038/nsmb.2284 Medline

17. D. Pogoryelov, O. Yildiz, J. D. Faraldo-Gómez, T. Meier, High-resolution structure of the rotor ring of a proton-dependent ATP synthase. *Nat. Struct. Mol. Biol.* **16**, 1068–1073 (2009). doi:10.1038/nsmb.1678 Medline

18. N. Mitome, S. Ono, H. Sato, T. Suzuki, N. Sone, M. Yoshida, Essential arginine residue of the F_o-I subunit in F_oF_1-ATP synthase has a role to prevent the proton shortcut without c-ring rotation in the F_o proton channel. *Biochem. J.* **430**, 171–177 (2010). doi:10.1042/BJ20100621 Medline

19. N. Klusch, B. J. Murphy, D. J. Mills, Ö. Yildiz, W. Kühlbrandt, Structural basis of proton translocation and force generation in mitochondrial ATP synthase. *eLife* **6**, e33274 (2017). doi:10.7554/eLife.33274 Medline

20. M. Allegretti, N. Klusch, D. J. Mills, J. Vonck, W. Kühlbrandt, K. M. Davies, Horizontal membrane-intrinsic α-helices in the stator *a*-subunit of an F-type ATP synthase. *Nature* **521**, 237–240 (2015). doi:10.1038/nature14185 Medline

21. V. Leone, J. D. Faraldo-Gómez, Structure and mechanism of the ATP synthase membrane motor inferred from quantitative integrative modeling. *J. Gen. Physiol.* **148**, 441–457 (2016). doi:10.1085/jgp.201611679 Medline

22. F. M. Assadi-Porter, R. H. Fillingame, Proton-translocating carboxyl of subunit *c* of F_1F_o H^+-ATP synthase: The unique environment suggested by the pK_a determined by ^{1}H NMR. *Biochemistry* **34**, 16186–16193 (1995). doi:10.1021/bi00049a034 Medline

23. M. J. Root, R. MacKinnon, Two identical noninteracting sites in an ion channel revealed by proton transfer. *Science* **265**, 1852–1856 (1994). doi:10.1126/science.7522344 Medline

24. J. A. Morrill, R. MacKinnon, Isolation of a single carboxyl-carboxylate proton binding site in the pore of a cyclic nucleotide-gated channel. *J. Gen. Physiol.* **114**, 71–84 (1999). doi:10.1085/jgp.114.1.71 Medline

25. T. K. Harris, G. J. Turner, Structural basis of perturbed pK_a values of catalytic groups in enzyme active sites. *IUBMB Life* **53**, 85–98 (2002). doi:10.1080/15216540211468 Medline

26. R. E. Koeppe II, R. M. Stroud, Mechanism of hydrolysis by serine proteases: Direct determination of the pK_a's of aspartyl-102 and aspartyl-194 in bovine trypsin using difference infrared spectroscopy. *Biochemistry* **15**, 3450–3458 (1976). doi:10.1021/bi00661a009 Medline

27. F. I. Valiyaveetil, R. H. Fillingame, On the role of Arg-210 and Glu-219 of subunit a in proton translocation by the *Escherichia coli* F_0F_1-ATP synthase. *J. Biol. Chem.* **272**, 32635–32641 (1997). doi:10.1074/jbc.272.51.32635 Medline

28. F. I. Valiyaveetil, R. H. Fillingame, Transmembrane topography of subunit a in the *Escherichia coli* F_1F_0 ATP synthase. *J. Biol. Chem.* **273**, 16241–16247 (1998). doi:10.1074/jbc.273.26.16241 Medline

29. J. Symersky, D. Osowski, D. E. Walters, D. M. Mueller, Oligomycin frames a common drug-binding site in the ATP synthase. *Proc. Natl. Acad. Sci. U.S.A.* **109**, 13961–13965 (2012). doi:10.1073/pnas.1207912109 Medline

30. U. P. John, P. Nagley, Amino acid substitutions in mitochondrial ATPase subunit 6 of *Saccharomyces cerevisiae* leading to oligomycin resistance. *FEBS Lett.* **207**, 79–83 (1986). doi:10.1016/0014-5793 (86)80016-3 Medline

31. I. G. Denisov, B. J. Baas, Y. V. Grinkova, S. G. Sligar, Cooperativity in cytochrome P450 3A4: Linkages in substrate binding, spin state, uncoupling, and product formation. *J. Biol. Chem.* **282**, 7066–7076 (2007). doi:10.1074/jbc.M609589200 Medline

32. R. B. Kapust, J. Tözsér, J. D. Fox, D. E. Anderson, S. Cherry, T. D. Copeland, D. S. Waugh, Tobacco etch virus protease: Mechanism of autolysis and rational design of stable mutants with wild-type catalytic proficiency. *Protein Eng.* **14**, 993–1000 (2001). doi:10.1093/protein/14.12.993 Medline

33. V. Pagadala, L. Vistain, J. Symersky, D. M. Mueller, Characterization of the mitochondrial ATP synthase from yeast *Saccharomyces cerevisae*. *J. Bioenerg. Biomembr.* **43**, 333–347 (2011). doi:10.1007/s10863-011-9364-5 Medline

34. U. Güldener, S. Heck, T. Fielder, J. Beinhauer, J. H. Hegemann, A new efficient gene disruption cassette for repeated use in budding yeast. *Nucleic Acids Res.* **24**, 2519–2524 (1996). doi:10.1093/nar/24.13.2519 Medline

35. N. Puri, J. Lai-Zhang, S. Meier, D. M. Mueller, Expression of bovine F_1-ATPase with functional complementation in yeast *Saccharomyces cerevisiae*. *J. Biol. Chem.* **280**, 22418–22424 (2005). doi:10.1074/jbc.M411113200 Medline

36. R. S. Sikorski, P. Hieter, A system of shuttle vectors and yeast host strains designed for efficient manipulation of DNA in *Saccharomyces cerevisiae*. *Genetics* **122**, 19–27 (1989). Medline

37. R. D. Gietz, R. A. Woods, Transformation of yeast by lithium acetate/single-stranded carrier DNA/polyethylene glycol method. *Methods Enzymol.* **350**, 87–96 (2002). doi:10.1016/S0076-6879 (02)50957-5 Medline

38. T. K. Ritchie, Y. V. Grinkova, T. H. Bayburt, I. G. Denisov, J. K. Zolnerciks, W. M. Atkins, S. G. Sligar, Chapter Eleven - Reconstitution of membrane proteins in phospholipid bilayer nanodiscs. *Methods Enzymol.* **464**, 211–231 (2009). doi:10.1016/S0076-6879 (09)64011-8 Medline

39. H. S. Penefsky, A centrifuged-column procedure for the measurement of ligand binding by beef heart F_1. *Methods Enzymol.* **56**, 527–530 (1979). doi:10.1016/0076-6879 (79)56050-9 Medline

40. X. Li, S. Zheng, D. A. Agard, Y. Cheng, Asynchronous data acquisition and on-the-fly analysis of dose fractionated cryoEM images by UCSFImage. *J. Struct. Biol.* **192**, 174–178 (2015). doi:10.1016/j.jsb.2015.09.003 Medline

41. W. Mi, Y. Li, S. H. Yoon, R. K. Ernst, T. Walz, M. Liao, Structural basis of MsbA-mediated lipopolysaccharide transport. *Nature* **549**, 233–237 (2017). doi:10.1038/nature23649 Medline

42. S. Q. Zheng, E. Palovcak, J.-P. Armache, K. A. Verba, Y. Cheng, D. A. Agard, MotionCor2: Anisotropic correction of beam-induced motion for improved cryo-electron microscopy. *Nat. Methods* **14**, 331–332 (2017). doi:10.1038/nmeth.4193 Medline

43. A. Rohou, N. Grigorieff, CTFFIND4: Fast and accurate defocus estimation from electron micrographs. *J. Struct. Biol.* **192**, 216–221 (2015). doi:10.1016/j.jsb.2015.08.008 Medline

44. H. Ru, M. G. Chambers, T.-M. Fu, A. B. Tong, M. Liao, H. Wu, Molecular mechanism of V(D)J recombination from synaptic RAG1-RAG2 complex structures. *Cell* **163**, 1138–1152 (2015). doi:10.1016/j.cell.2015.10.055 Medline

45. S. H. Scheres, RELION: Implementation of a Bayesian approach to cryo-EM structure determination. *J. Struct. Biol.* **180**, 519–530 (2012). doi:10.1016/j.jsb.2012.09.006 Medline

46. X. C. Bai, E. Rajendra, G. Yang, Y. Shi, S. H. Scheres, Sampling the conformational space of the catalytic subunit of human γ-secretase. *eLife* **4**, e11182 (2015). doi:10.7554/eLife.11182 Medline

47. P. Emsley, K. Cowtan, Coot: Model-building tools for molecular graphics. *Acta Crystallogr. D Biol. Crystallogr.* **60**, 2126–2132 (2004). doi:10.1107/S0907444904019158 Medline

48. G. N. Murshudov, P. Skubák, A. A. Lebedev, N. S. Pannu, R. A. Steiner, R. A. Nicholls, M. D. Winn, F. Long, A. A. Vagin, REFMAC5 for the refinement of macromolecular crystal structures. *Acta Crystallogr. D Biol. Crystallogr.* **67**, 355–367 (2011). doi:10.1107/S0907444911001314 Medline

49. P. D. Adams, P. V. Afonine, G. Bunkóczi, V. B. Chen, I. W. Davis, N. Echols, J. J. Headd, L.-W. Hung, G. J. Kapral, R. W. Grosse-Kunstleve, A. J. McCoy, N. W.

Moriarty, R. Oeffner, R. J. Read, D. C. Richardson, J. S. Richardson, T. C. Terwilliger, P. H. Zwart, PHENIX: A comprehensive Python-based system for macromolecular structure solution. *Acta Crystallogr. D Biol. Crystallogr.* **66**, 213–221 (2010). doi:10.1107/S0907444909052925 Medline

50. B. A. Barad, N. Echols, R. Y.-R. Wang, Y. Cheng, F. DiMaio, P. D. Adams, J. S. Fraser, EMRinger: Side chain-directed model and map validation for 3D cryo-electron microscopy. *Nat. Methods* **12**, 943–946 (2015). doi:10.1038/nmeth.3541 Medline

51. V. B. Chen, W. B. Arendall III, J. J. Headd, D. A. Keedy, R. M. Immormino, G. J. Kapral, L. W. Murray, J. S. Richardson, D. C. Richardson, MolProbity: All-atom structure validation for macromolecular crystallography. *Acta Crystallogr. D Biol. Crystallogr.* **66**, 12–21 (2010). doi:10.1107/S0907444909042073 Medline

52. J. C. Phillips, R. Braun, W. Wang, J. Gumbart, E. Tajkhorshid, E. Villa, C. Chipot, R. D. Skeel, L. Kalé, K. Schulten, Scalable molecular dynamics with NAMD. *J. Comput. Chem.* **26**, 1781–1802 (2005). doi:10.1002/jcc.20289 Medline

53. R. B. Best, X. Zhu, J. Shim, P. E. M. Lopes, J. Mittal, M. Feig, A. D. Mackerell Jr., Optimization of the additive CHARMM all-atom protein force field targeting improved sampling of the backbone φ, ψ and side-chain χ_1 and χ_2 dihedral angles. *J. Chem. Theory Comput.* **8**, 3257–3273 (2012). doi:10.1021/ct300400x Medline

54. J. B. Klauda, R. M. Venable, J. A. Freites, J. W. O'Connor, D. J. Tobias, C. Mondragon-Ramirez, I. Vorobyov, A. D. MacKerell Jr., R. W. Pastor, Update of the CHARMM all-atom additive force field for lipids: Validation on six lipid types. *J. Phys. Chem. B* **114**, 7830–7843 (2010). doi:10.1021/jp101759q Medline

55. L. Huang, B. Roux, Automated force field parameterization for non-polarizable and polarizable atomic models based on ab initio target data. *J. Chem. Theory Comput.* **9**, 3543–3556 (2013). doi:10.1021/ct4003477 Medline

56. R. Staritzbichler, C. Anselmi, L. R. Forrest, J. D. Faraldo-Gómez, GRIFFIN: A versatile methodology for optimization of protein-lipid interfaces for membrane protein simulations. *J. Chem. Theory Comput.* **7**, 1167–1176 (2011). doi:10.1021/ct100576m Medline

57. W. Zhou, V. Leone, A. Krah, J. D. Faraldo-Gómez, Predicted structures of the proton-bound membrane-embedded rotor rings of the *Saccharomyces cerevisiae* and *Escherichia coli* ATP synthases. *J. Phys. Chem. B* **121**, 3297–3307 (2017). doi:10.1021/acs.jpcb.6b08051 Medline

58. J. S. Papadopoulos, R. Agarwala, COBALT: Constraint-based alignment tool for multiple protein sequences. *Bioinformatics* **23**, 1073–1079 (2007). doi:10.1093/bioinformatics/btm076 Medline

59. The PyMOL Molecular Graphics System, version 2.0, Schrödinger, LLC.